Editors' Suggestion

Increased lifetime of metastable skyrmions by controlled doping

M. T. Birch,[1,2] R. Takagi,[3] S. Seki,[3] M. N. Wilson,[1] F. Kagawa,[3,4] A. Štefančič,[5] G. Balakrishnan,[5] R. Fan,[2] P. Steadman,[2] C. J. Ottley,[6] M. Crisanti,[5,7] R. Cubitt,[7] T. Lancaster,[1] Y. Tokura,[3,4] and P. D. Hatton[1]

[1]*Centre for Materials Physics, Durham University, Durham DH1 3LE, United Kingdom*
[2]*Diamond Light Source, Didcot OX11 0DE, United Kingdom*
[3]*RIKEN Center for Emergent Matter Science, Wako 351-0198, Japan*
[4]*Department of Applied Physics, University of Tokyo, Bunkyo-ku 113-8656, Japan*
[5]*Department of Physics, University of Warwick, Coventry CV4 7AL, United Kingdom*
[6]*Earth Sciences, Durham University, Durham DH1 3LE, United Kingdom*
[7]*Institut Laue-Langevin, CS 20156, 38042 Grenoble Cedex 9, France*

(Received 29 November 2018; revised manuscript received 11 June 2019; published 22 July 2019)

Previous observations of metastable magnetic skyrmions have shown that close to the equilibrium pocket the metastable state has a short lifetime, and therefore, rapid cooling is required to generate a significant skyrmion population at low temperatures. Here, we report that the lifetime of metastable skyrmions in crystals of Cu_2OSeO_3 is extended by a factor of 50 with the introduction of only 2.5% zinc doping, allowing over 50% of the population to survive when field cooling at a rate of just 1 K/min. Our systematic study suggests that the lifetime enhancement is due to the increase in the pinning site density, rather than an alteration to the energy barrier of the decay process. We expect that doping can be exploited to control the lifetime of the metastable SkL state in other chiral magnets, offering a method of engineering skyrmion materials towards application in future devices.

DOI: 10.1103/PhysRevB.100.014425

I. INTRODUCTION

The magnetic skyrmion lattice (SkL) is an example of a state of matter protected by a topological energy barrier [1]. This barrier arises from the inability to continuously transform between spin structures with different topological charges N [2]. This number effectively counts the number of times the spin direction wraps around a unit sphere, yielding $N = 1$ for the skyrmion state and $N = 0$ for the competing, topologically trivial, helical, conical, and uniformly magnetized magnetic states. The resulting energy barrier stabilizes the skyrmion state, protecting it from destruction by small perturbations that cause continuous deformations in the spin structure but not from discontinuous changes, which may be caused by large thermal fluctuations.

In bulk materials, skyrmions are typically observed in chiral systems such as the B20 structures MnSi [3,4], $Fe_{0.5}Co_{0.5}Si$ [5,6], and FeGe [7,8] (space group $P2_13$), where the broken inversion symmetry results in an antisymmetric Dzyaloshinskii-Moriya interaction which favors canting between neighboring spins. The competition of this interaction with the ferromagnetic exchange and Zeeman interactions produces noncolinear spin textures such as the helical and conical states. In the presence of thermal fluctuations near T_c [1], at particular values of crystal anisotropies [9], or with the addition of magnetic frustration [10], the magnetic SkL state is energetically favored, forming a skyrmion lattice in a plane perpendicular to the direction of an applied magnetic field. In bulk materials, this lattice has an extended, stringlike structure in the field direction, as illustrated in Fig. 1(a) [11]. Other skyrmion-hosting chiral magnets include β-Mn-type Co-Zn-Mn [12] alloys ($P4_132$), with T_c above 300 K, and the multiferroic Cu_2OSeO_3 [13] ($P2_13$), the target material of the present study.

The extensive study of skyrmions has in part been motivated by the observation that they can be moved with low current densities [14], giving skyrmions prospective applications in future high-density, ultralow-power memory devices. In such devices, skyrmions are required to exist at room temperature and zero applied magnetic field, ensuring the preservation of any stored data while the device is unpowered. The limited extent of the equilibrium SkL phase in temperature and applied field therefore presents a significant obstacle which must be overcome. Metastable skyrmions, which have now been observed in the Co-Zn-Mn alloys [15–17], MnSi [18–20], $Fe_{0.5}Co_{0.5}Si$ [5,21], and Cu_2OSeO_3 [9,22,23], offer distinct advantages as candidates for device application. They are observed to exist over a greatly extended field and temperature range, including at zero field and room temperature in $Co_9Zn_9Mn_2$ [16]. Moreover, the reading of metastable skyrmions and writing using rapid temperature control via current pulses have already been demonstrated [18]. However, their utility depends upon two crucial factors: the metastable SkL state must have a lifetime long enough to prevent data degradation, and the writing process must reliably produce skyrmions at feasible cooling rates.

Previous work has suggested that metastable skyrmion strings unwind by the proliferation and subsequent motion of magnetic Bloch points, which form where skyrmion strings either merge together or break in two, as illustrated in Fig. 1(a) (1 and 2). Current understanding suggests that the merging and breaking processes occur when the SkL state transforms into the helical [21] and conical states [20], respectively. These Bloch points act as sources or sinks of topological charge, allowing the skyrmion tubes to unwind into the competing topologically trivial states [24].

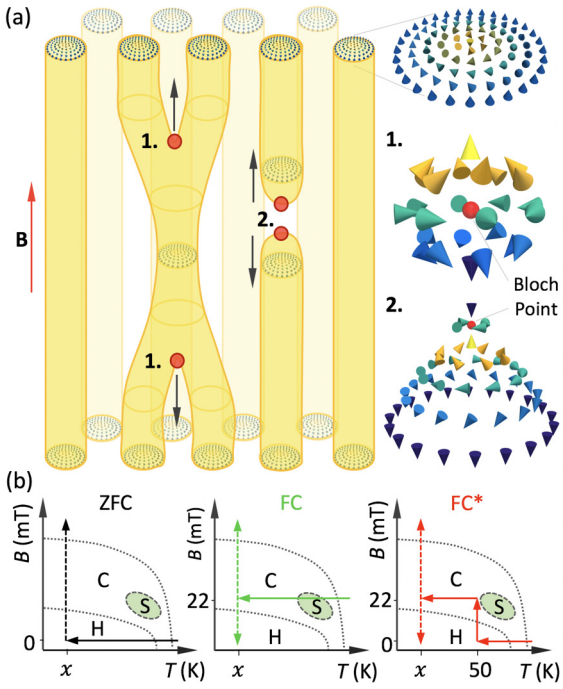

FIG. 1. (a) Illustration of the vertical, stringlike structure of a hexagonal lattice of Bloch skyrmions. Two scenarios for the Bloch point unwinding mechanism are displayed. (b) Schematic diagrams of the zero-field-cooling (ZFC; black) and field-cooling (FC and FC*; green and red) measurement procedures. Solid lines indicate the cooling procedure, while dashed lines indicate the measurement path. Dotted lines illustrate the boundaries between the helical (H), conical (C), and skyrmion (S) phases.

By comparing metastable skyrmions in the disordered CoZnMn alloys [10,15] and $Fe_{0.5}Co_{0.5}Si$ [5] to those in MnSi, it has been speculated that a key factor in the lifetime of the metastable state is that the Bloch points are strongly pinned by defects and disorder present in the underlying crystal lattice. These Bloch points propagate only by thermally assisted creep motion [20] in a manner similar to the propagation of magnetic domain walls [25–28]. It has also been suggested that a similar effect may hinder the helical reorientation process in Ga- and Ir-doped MnSi [29]. This effect offers a potential route to engineer the lifetime of metastable skyrmions via doping. In the present work, we systematically study and quantify this effect by investigating a series of Cu_2OSeO_3 crystals doped with nonmagnetic Zn ions. Our detailed time-resolved AC susceptibility measurements reveal that even a small quantity of Zn both dramatically increases the lifetime and substantially reduces the cooling rate required for the formation of the metastable SkL state.

II. METHODS

Pristine and Zn-doped Cu_2OSeO_3 single crystals were grown from presynthesized polycrystalline powders using the chemical vapor transport technique, as detailed in previous work [30]. The elemental composition of the crystals was measured by inductively coupled plasma mass spectroscopy (ICP-MS). Known masses (∼1–5 mg) of each crystal were dissolved in high-purity nitric acid (Romil-SpA) and diluted with high-purity water. The resulting solutions were then analyzed using an X-Series 2 ICP-MS (Thermo Scientific), considering all naturally occurring isotopes of Cu, Zn, and Se to monitor the possible presence of impurity elements and polyatomic species. These measurements revealed the actual Zn substitution levels of the crystals selected for this study to be $2.8\% \pm 0.1\%$, $2.5\% \pm 0.2\%$, $1.0\% \pm 0.2\%$, and $0.0\% \pm 0.1\%$.

To identify the presence of metastable skyrmions, three contrasting field-temperature procedures were employed: zero field cooling (ZFC), field cooling (FC), and field cooling around the equilibrium SkL state (FC*), as illustrated in Fig. 1(b). In the ZFC procedure, the sample was cooled from 70 K down to the final temperature in zero applied magnetic field (solid black arrow). In the FC procedure, the sample was cooled in a field of 22 mT, from 70 K, through the equilibrium SkL state, down to the final temperature (solid green arrow). In the FC* procedure, the sample was cooled at 0 mT from 70 to 50 K. A field of 22 mT was then applied, and the sample was cooled down to the final temperature (solid red arrows). After initializing the magnetic configuration of the sample with these procedures, measurements were performed with isothermal field sweeps (dashed black, green, and red arrows). The single-crystal samples were aligned with the magnetic field applied along the [111] direction for all measurements.

Magnetometry measurements were recorded using a superconducting quantum interference device magnetometer (MPMS3, Quantum Design), furnished with the optional AC magnetometry option. All AC susceptibility measurements were performed at a frequency of 10 Hz and an amplitude of 0.1 mT. The single-crystal samples were mounted on a quartz rod with GE varnish and positioned inside the vacuum chamber. The T_c of each sample was measured with magnetization versus temperature measurements and was found to be 55.4 ± 0.1, 56.2 ± 0.1, 57.4 ± 0.1, and 58.8 ± 0.1 K for the 2.8%, 2.5%, 1.0%, and 0.0% Zn-doped samples. Magnetization versus field measurements determined that the value of the saturation magnetization was reduced with the addition of nonmagnetic zinc ions, confirming that the Zn ions were substituted on to the Cu lattice sites [30].

The broadband microwave absorption spectroscopy was carried out by using a vector network analyzer, with the single-crystal sample mounted on a coplanar waveguide as described in previous work [31]. At each temperature, the spectrum of microwave absorption caused by magnetic resonance, $\Delta S_{12}(\nu) = S_{12}(\nu) - S_{12}^{\mathrm{ref}}(\nu)$, was derived by subtraction of the common background $S_{12}^{\mathrm{ref}}(\nu)$ from the raw transmittance spectrum $S_{12}(\nu)$. Here, a spectrum measured at an applied field of 250 mT was adopted as the reference spectrum $S_{12}^{\mathrm{ref}}(\nu)$; at this field, the magnetic resonance was absent within our target frequency range from 1 to 6 GHz.

The small-angle neutron scattering (SANS) measurements were performed on the D33 instrument at the Institut Laue-Langevin (ILL). The Cu_2OSeO_3 single crystal was mounted on a 200-μm-thick aluminum plate, positioned inside a "Blue Charlie" superconducting magnet helium flow cryostat, and aligned with the neutron beam. Measurements were performed with a neutron wavelength of 10 Å and a collimation distance of 12 m. SANS patterns shown are the sum of

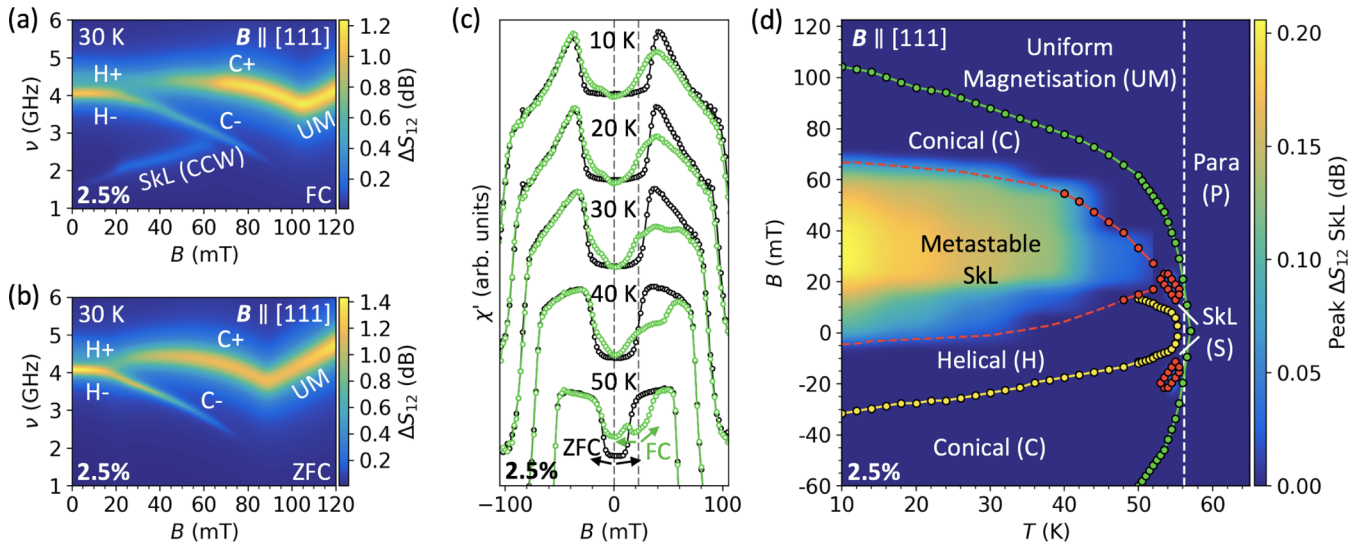

FIG. 2. (a) and (b) Microwave absorption spectra measured in the 2.5% sample as a function of applied magnetic field after the FC and ZFC processes, respectively. Magnetic resonances associated with the helical (H±), conical (C±), and uniformly magnetized (UM) spin structures are labeled. In (a), the counterclockwise (CCW) skyrmion lattice (SkL) mode is observed. (c) AC susceptibility measurements performed on the 2.5% sample after FC (green) and ZFC (black) processes. (d) The magnetic phase diagram of the 2.5% Zn-doped sample measured after FC measurements. The color map shows the strength of the SkL CCW mode measured in the microwave absorption measurements at each temperature and field. The colored dots show the SkL (red), helical-conical (yellow), and conical-uniformly-magnetized (green) phase boundaries, as determined by AC susceptibility measurements.

measurements performed in a rocking curve, achieved by rotating the angle of the field and sample relative to the neutron beam by ±5° and measuring for 1 min every 0.5°.

III. IDENTIFYING METASTABLE SKYRMIONS

Microwave absorption spectra, measured as a function of applied field after FC and ZFC to 30 K, are displayed in Figs. 2(a) and 2(b), respectively. In this technique, microwaves are absorbed at the characteristic resonant frequencies of the magnetic structures present in the sample [31–34]. Absorption peaks belonging to the helical (H±), conical (C±), and uniformly magnetized (UM) magnetic structures are observed in the response of the sample after both FC and ZFC procedures. However, there is an additional absorption mode with positive B slope in the FC data which we ascribe to the counterclockwise (CCW) resonance of the metastable skyrmion lattice [22,35]. AC susceptibility χ' measured at a range of temperatures for both FC and ZFC procedures is shown in Fig. 2(c). There is a clear depression in the measured value of χ' around 22 mT after the FC process, which is consistent with the χ' signal observed for the equilibrium SkL state [36–38] (see the Appendix, Fig. 6). Therefore, we attribute this difference to the presence of the metastable SkL state. Results from these two techniques are summarized in the magnetic phase diagram in Fig. 2(d), which demonstrates the large extent of the metastable SkL phase, compared to the smaller equilibrium phase (S; see the Appendix). Here, the color map plots the peak absorption of the CCW SkL resonance measured at each field and temperature, while the colored dots indicate the boundaries of the magnetic phases as determined by AC susceptibility measurements.

SANS measurements were employed to confirm our identification of the metastable SkL state. These measurements were performed on a larger 2.8% Zn-doped sample. The experimental setup is displayed in Fig. 3(a). Figure 3(b) illustrates the location of the SkL and conical magnetic peaks in reciprocal space, demonstrating that the wave vectors of the SkL and the conical states point perpendicular and parallel to the applied magnetic field, respectively [39]. With the magnetic field applied along the [111] crystal axis and parallel to the neutron beam, Fig. 3(c) displays the sixfold-symmetric pattern characteristic of the hexagonal equilibrium SkL at 54 K, as indicated by the blue circle in Fig. 3(b), with a skyrmion spacing of 63 ± 4 nm. The error indicates the distribution of spacings present in the sample, calculated from the width of the SkL peak in the q direction. Figure 3(d) shows the SANS pattern recorded after FC down to 5 K. The resulting sixfold pattern confirms the survival of the metastable SkL state at low temperatures, with a spacing of 63 ± 4 nm. Figure 3(e) demonstrates the absence of a sixfold pattern at 22 mT after the ZFC procedure to 5 K, indicating no skyrmions are present. Here, the magnetic state is expected to consist of helices aligned to the [100] crystalline axes. However, as no [100] directions are perpendicular to the neutron beam, we observe no diffraction intensity. Finally, Fig. 3(f) displays the SANS pattern measured after FC to 5 K with the magnetic field applied perpendicular to the neutron beam. Here, the vertical diffraction peaks demonstrate the presence of domains of the metastable SkL, while the horizontal peaks indicate the coexistence of competing conical domains, as indicated by the green circle in Fig. 3(b).

IV. LIFETIME OF METASTABLE SKYRMIONS

Once formed, the population of metastable skyrmions $S(t)$ has been observed to follow a decay modeled by a stretched exponential [16], with a temperature-dependent lifetime

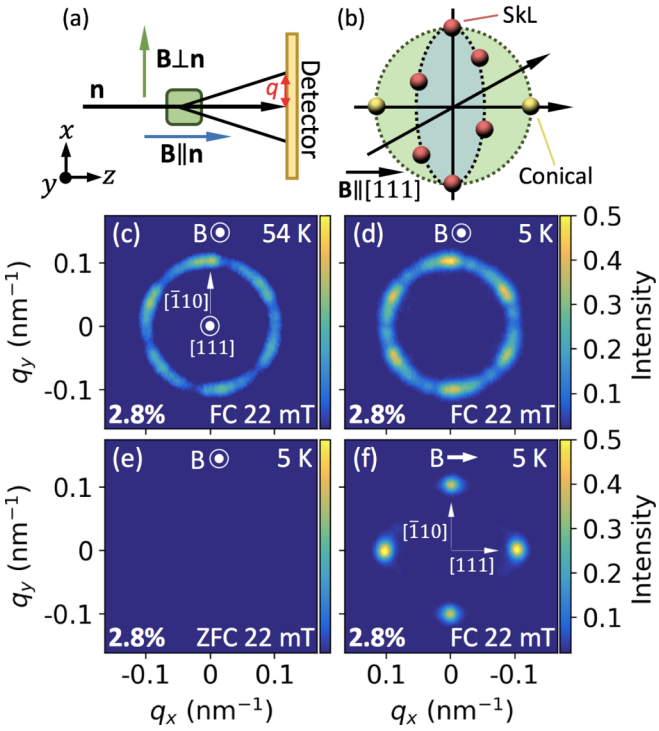

FIG. 3. (a) Schematic diagram of the experimental setup of the small-angle neutron scattering (SANS) measurements, indicating the orientations of the magnetic field with the neutron beam **n**. (b) Illustration of the locations of the skyrmion (red) and conical (yellow) peaks in reciprocal space. The blue and green circles indicate the peaks observed when the field is parallel and perpendicular to the neutron beam. (c)–(f) SANS diffraction patterns recorded at selected temperatures, after both (c), (d), and (f) field-cooling and (e) zero-field-cooling procedures, with the applied magnetic field (c)–(e) parallel and (f) perpendicular to the incident neutron beam.

$\tau(T)$. During this decay process, the real part of the AC susceptibility χ' relaxes from its value in the skyrmion state to the value in the conical state (see the Appendix, Fig. 6). Assuming that changes in the value of χ' are proportional to changes in the skyrmion population, the time dependence of the normalized AC susceptibility χ'_N can be modeled with a stretched exponential function (see the Appendix for details),

$$\chi'_N(t) = -\exp\left[-\left(\frac{t}{\tau(T)}\right)^{\beta}\right]. \tag{1}$$

Utilizing this expression and time-resolved measurements of χ'_N, as shown in Figs. 4(a)–4(c), the lifetime of the metastable state was measured as a function of temperature for each Zn-doped crystal. The fitted lifetime was then converted to the mean lifetime for a stretched exponential function [40]. Figure 4(e) displays the measured values of $\tau(T)$ for each crystal, plotted as a function of $T - T_s$, where T_s is the lowest-temperature extent of the equilibrium skyrmion state, taken as 4 K below T_c for all crystals. It is evident that for a given $T - T_s$, the 2.5% crystal has a lifetime longer by a factor of ~50 when compared to the 0% crystal.

The relationship between the lifetime of the metastable SkL state and the temperature of the sample allows us to model the measured lifetimes using Arrhenius's law [18],

$$\tau(T) = \tau_0 \exp\left[\frac{E_b}{k_B T}\right] = \tau_0 \exp\left[a\frac{(T_s - T)}{T}\right]. \tag{2}$$

Here, the typical activation energy term has been replaced with the energy barrier E_b protecting the metastable SkL. As the sample approaches T_s, the height of E_b and therefore the lifetime are reduced. For the SkL to conical transition, the temperature dependence of the energy barrier can be approximated as $E_b/k_B = a(T_s - T)$, with a being the linear proportional constant [18]. Using this framework and the model of skyrmion strings unwinding via Bloch point formation and motion, we present two possible ways in which the lifetime of the metastable SkL state can be increased with doping, as depicted in Fig. 4(d). In scenario 1, the value of a is increased, corresponding to an increase in the energy barrier which must be overcome to unwind the skyrmion state. In scenario 2, the value of τ_0 is increased, which is typically considered to be an attempt frequency. An important component of this prefactor is an entropic correction, which concerns the available pathways across an activation barrier and has previously been shown to play an important role in the stability of the metastable skyrmion state [24,41].

We utilize equation (2) to fit the data sets in Fig. 4(e) and extract the gradient, a, and the intercept, τ_0, for each crystal. Figure 4(f) displays these fitted parameters, plotted as a function of Zn-doping level. It is clear that a is constant across all the crystals within experimental uncertainty, with an average value of 97 ± 3, which corresponds to an E_b/k_B of $\sim 5 \times 10^3$ K at 0 K. The energy barrier height is therefore not substantially altered by the introduction of zinc ions. In contrast, τ_0, plotted on the secondary, logarithmic axis of Fig. 3(f), exhibits a nonlinear increase with Zn doping, with values of 412 ± 140, 22 ± 11, and 8 ± 2 s for the 2.5%, 1.0%, and 0.0% crystals, respectively. The magnetic structure of Cu_2OSeO_3 is composed of tetrahedra formed of four ferrimagnetically ordered Cu spins, which act as a single spin [42,43]. The substitution of a Zn ion into this cluster can be expected to reduce the overall magnitude of the spin [30], acting as a magnetic impurity, or pinning site. It has previously been suggested that the motion of Bloch points in the unwinding process would be strongly pinned by any impurities present in the material [21]. The increase in τ_0 could therefore be understood as an increase in the density of these pinning sites with Zn doping, leading to a longer lifetime without altering the energy barrier of the decay process.

The fraction of metastable skyrmions which survives after FC S_0 is related to the cooling rate k. Because the lifetime of the metastable SkL state is shortest just below T_s, cooling through this region slowly results in a considerable loss of skyrmion population. We investigated this relationship by measuring χ' after FC at a range of k between 0.5 and 40 K/min. The results for the 2.5% and 0.0% crystals, measured 10 K below T_s, are plotted in Figs. 5(a) and 5(b), respectively (blue and yellow points). These measurements are contrasted with data measured after the ZFC (black) and FC* (red) procedures. We assume that the difference in χ' between the FC and FC* processes, $\Delta\chi' = \chi'_{FC^*} - \chi'_{FC}$, is proportional to the population of metastable skyrmions. In Fig. 5(c), the measured value of $\Delta\chi'$ at 22 mT is plotted as

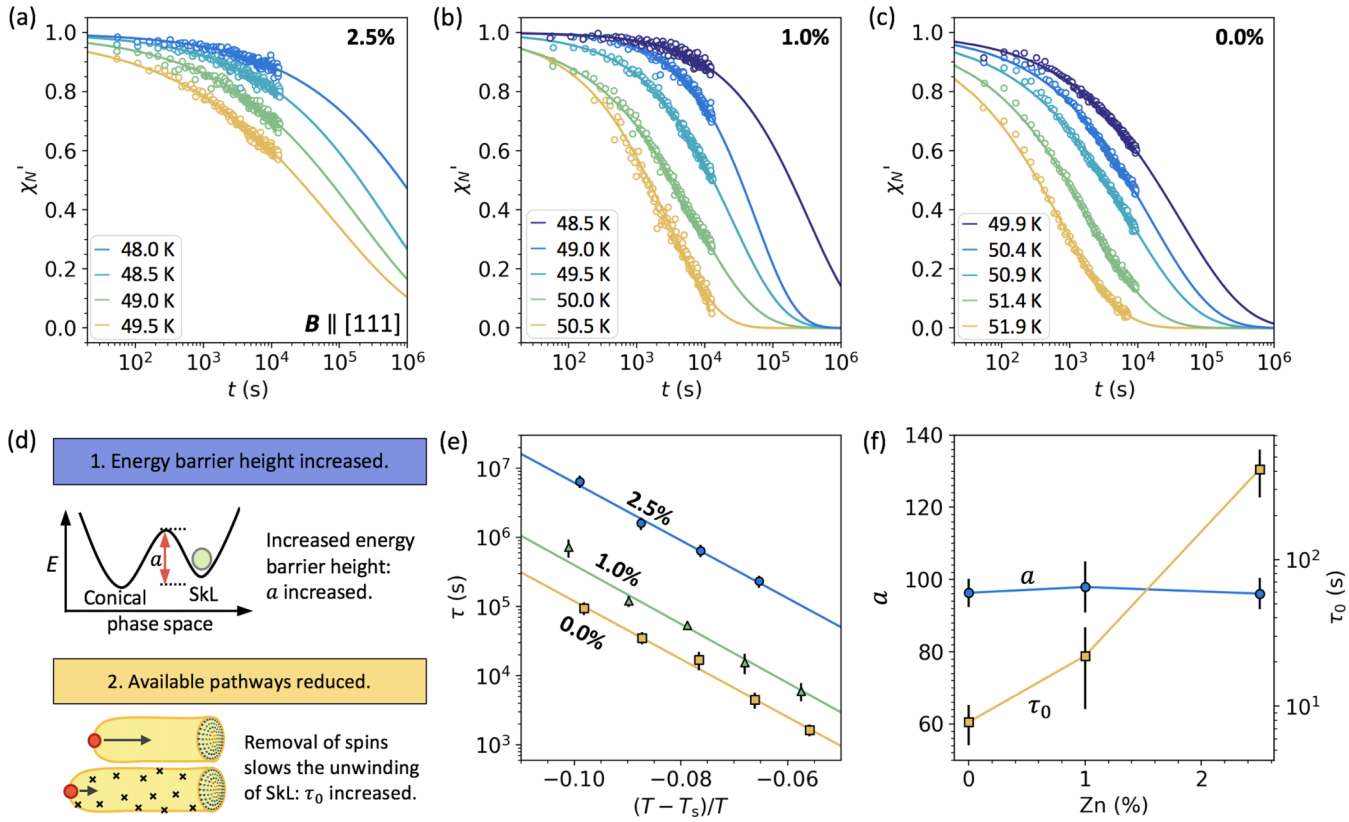

FIG. 4. (a)–(c) Normalized, time-resolved AC susceptibility measurements at a range of temperatures for the 2.5%, 1.0%, and 0.0% crystals, respectively. The data sets are fitted with stretched exponential functions. (d) Schematic representations of the two possible scenarios for increasing the lifetime of metastable skyrmions, based on arguments from Arrhenius's law. (e) The extracted lifetimes from (a)–(c) plotted as a function of $(T - T_s)/T$ and fitted with Arrhenius's law, determining values for τ_0 and a. (f) The fitted a and τ_0 parameters are plotted as a function of the Zn-doping level.

a function of cooling rate for all three crystals. For all cooling rates, the value of $\Delta\chi'$ in the 2.5% crystal is far greater than that of the 0.0% crystal, and we therefore infer that the population of metastable skyrmions is substantially higher.

In order to estimate the metastable skyrmion population in each sample from this experimental data, we calculated the expected metastable skyrmion population loss during FC. Our derivation (see the Appendix) yields an expression for the metastable population after cooling from T_s to the final temperature T_f at a rate of k,

$$S_0 = S_i \exp\left[\int_{T_s}^{T_f} \frac{-\beta}{T - T_s}\left(\frac{T - T_s}{k\tau_0 \exp\left[a\frac{T_s - T}{T}\right]}\right)^{\beta} dT\right], \quad (3)$$

where S_i is the initial skyrmion population before cooling. We use this model and the values for β, a, and τ_0 fitted for each crystal in Fig. 4 to simulate the evolution of the skyrmion population as a function of temperature for cooling rates between 0.5 and 40 K/min. The results for the 2.5% and 0.0% crystals are displayed in Figs. 5(d) and 5(e). It is clear that the largest population loss occurs in the first ∼2 K below T_s, after which the long lifetime effectively locks in the population. The final calculated metastable skyrmion population S_0/S_i for each crystal at $T - T_s = 10$ K is plotted as a function of k in Fig. 5(f). The strong qualitative agreement between the experimental data in Fig. 5(c) and the simulated model in Fig. 5(f) suggests that the Arrhenius model for $\tau(T)$ is valid and that $E_b/k_B = a(T_s - T)$ is a reasonable assumption for the relationship between energy barrier and temperature. Together, these plots indicate that although a cooling rate as high as 40 K/min cannot achieve a metastable population of ∼50% in the 0.0% crystal, this is achieved at a cooling rate of just 1 K/min in the 2.5% crystal.

We have shown that doping Zn ions onto the Cu sites in Cu_2OSeO_3 crystals increases the lifetime of the metastable SkL state. As a result, the cooling rate required to achieve a substantial metastable population when field cooling is greatly reduced. Our analysis of lifetimes measured as a function of temperature suggests that an increased density of pinning sites caused by the substitution of magnetic Cu ions with nonmagnetic Zn ions is responsible for this increased lifetime, rather than an alteration of the energy barrier. This slows the motion of the Bloch points responsible for the skyrmion decay process. We expect that this effect can be exploited to engineer the metastable SkL lifetime in other doped skyrmion-hosting systems.

Data presented in this paper will be made available via the Durham University data depository [47].

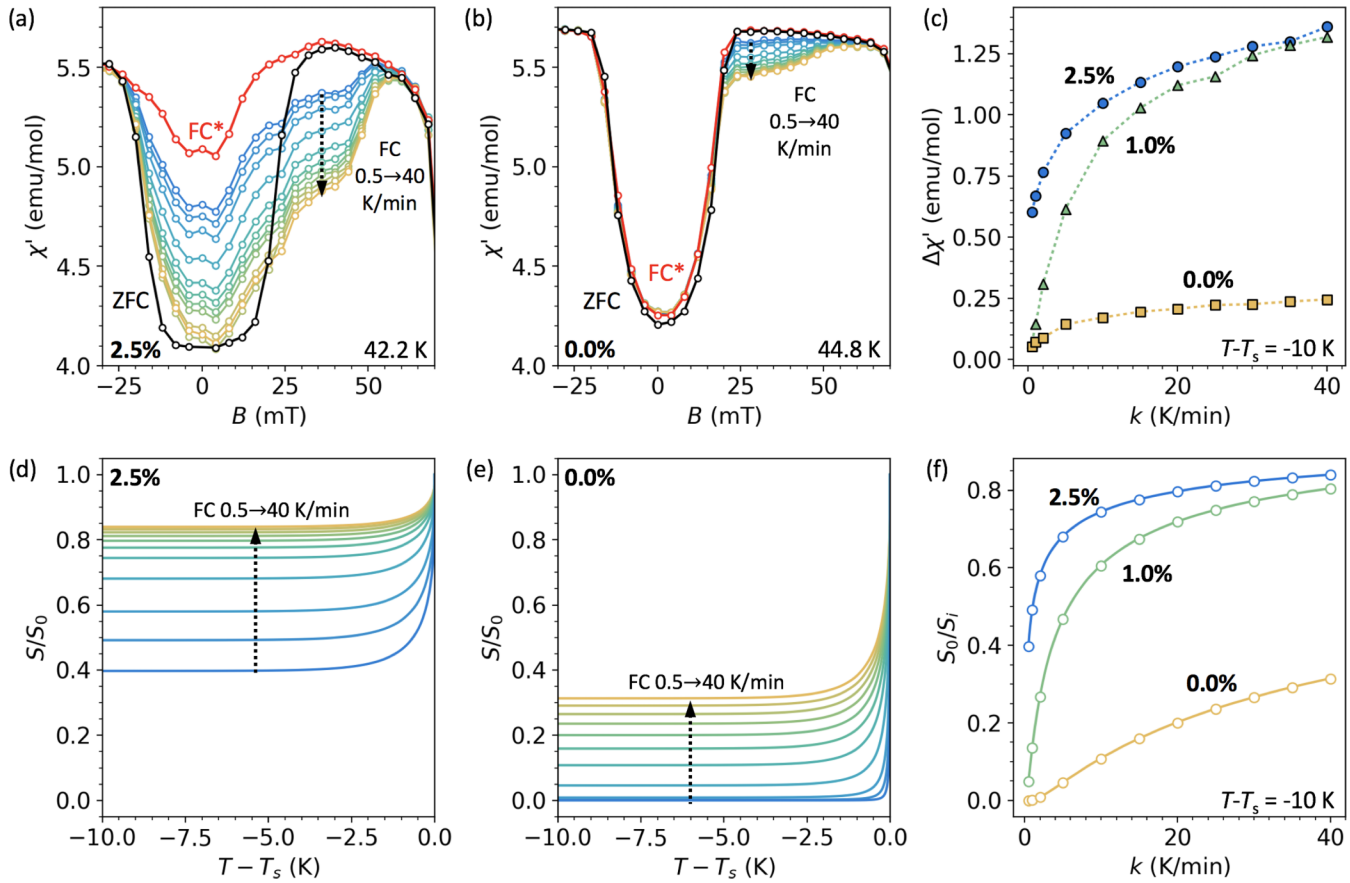

FIG. 5. (a) and (b) AC susceptibility χ' plotted as a function of applied magnetic field for the 2.5% and 0.0% Zn-doped samples, respectively, measured after ZFC (black) and FC* (red) procedures at 10 K below T_s. Multiple FC data sets are also shown, measured after different cooling rates between 0.5 K/min (blue) and 40 K/min (yellow). (c) The difference between the FC and FC* χ' data $\Delta\chi'$ measured at 22 mT in all samples, plotted as a function of cooling rate. (d) and (e) The simulated evolution of the metastable skyrmion population for the 2.5% and 0.0% crystals, plotted as a function of temperature below T_s at different cooling rates, calculated using values for a and τ_0 from Fig. 4. (f) The final simulated population of metastable skyrmions at 10 K below T_s, plotted as a function of cooling rate for all three samples. The circles show the simulated values at the same cooling rates measured in (c).

ACKNOWLEDGMENTS

The authors would like to thank K. Franké and T. Hicken for valuable discussions about the work. We are also grateful to M. Sussmuth at the I10 beamline, Diamond Light Source. This work was supported by the U.K. Skyrmion Project EPSRC Programme Grant (Grant No. EP/N032128/1), ILL Proposal No. 5-41-982, and the JSPS Summer Program 2017 in collaboration with SOKENDAI, who funded M.T.B.'s placement at RIKEN, Japan. S.S. was supported by Grants-in-Aid for Scientific Research (A) (Grant No. 18H03685) and a Grant-in-Aid for Scientific Research on Innovative Area, "Nano Spin Conversion Science" (Grant No. 17H05186) from JSPS and PRESTO from JST. M.N.W. acknowledges the support of the Natural Sciences and Engineering Research Council of Canada (NSERC).

APPENDIX

Figure 6(a) displays one of the microwave absorption spectra used to plot the phase diagram in Fig. 2(d) for the 2.5% sample. After FC at 22 mT to 30 K, absorption spectra were measured between −20 and 120 mT, $\Delta S_{12}(\nu)$. After the background subtraction, each spectrum was fitted using multiple Lorentzian peaks (colored lines). This is demonstrated in the spectra plotted alongside each color map, which displays the data (black) along with the fitted Lorentzian peaks. Figure 6(b) displays the microwave spectra when measuring a field sweep at 54 K, passing through the equilibrium SkL phase, again fitted with Lorentzian peaks. At this temperature, the H± and C± resonances are indistinguishable. The fitted peak height of the CCW SkL resonance at each temperature and field was used to plot the color map in Fig. 2(d).

Figures 6(c) and 6(d) display AC susceptibility data measured at 54 and 48 K, respectively, in the 2.5% sample after both FC (green line) and ZFC (black line), showing a comparison between the AC signal measured for the equilibrium and metastable SkL states. In Fig. 6(d), the red arrow indicates how the AC susceptibility $\chi'(t)$ relaxes as the metastable SkL state decays into the conical state with time. The time evolution of the metastable skyrmion population follows a stretched exponential function,

$$S(t) = S_0 \exp\left[-\left(\frac{t}{\tau(T)}\right)^{\beta}\right]. \quad \text{(A1)}$$

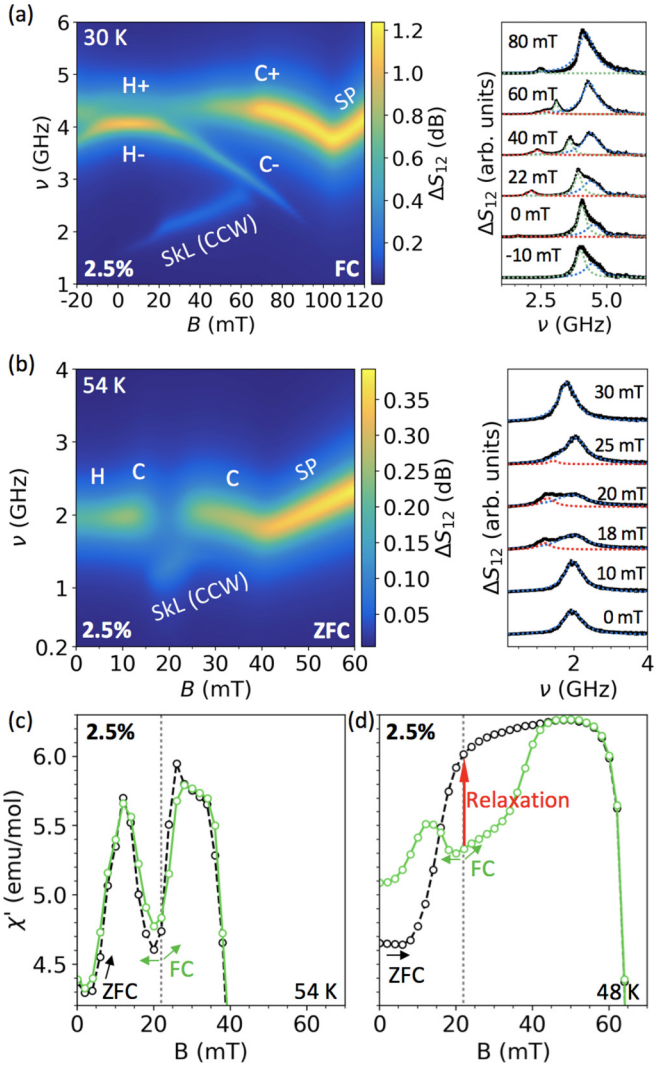

FIG. 6. (a) Microwave absorption spectra measured on the 2.5% sample as a function of field at 30 K after FC (left panel). Individual spectra measured at each field, with peaks belonging to the metastable SkL (red), H/C− (green), and H/C+ (blue) resonances fitted with Lorentzian functions (right). (b) Microwave spectra recorded as a function of field after ZFC to 54 K (left). The CCW SkL peak here is the equilibrium SkL phase. Peaks belonging to the SkL (red) and H/C (blue) resonances are fitted with Lorentzian functions (right). (c) and (d) AC susceptibility χ' measured as a function of applied magnetic field after ZFC (black) and FC (green) at 54 and 48 K, respectively, in the 2.5% crystal. The expected relaxation of χ' as the metastable SkL decays is illustrated by the red arrow.

Assuming that changes in $\chi'(t)$ are proportional to changes in $S(t)$, we can model the evolution of the AC susceptibility data with Eq. (1). In the main text, the AC susceptibility is normalized, $\chi'_N = [\chi'_f - \chi'(t)]/(\chi'_f - \chi'_0)$, where χ_0 is the initial value of χ' at $t = 0$ and χ_f is the value the system is tending to as $t \to \infty$. In the analysis of the lifetime measurements, we fixed χ_0 to the value of the first measured data point after temperature stabilization. We fixed χ_f to the value of χ measured at the same field and temperature after the FC* procedure, which we argue gives a reasonable value for the system after it has fully relaxed to the conical state.

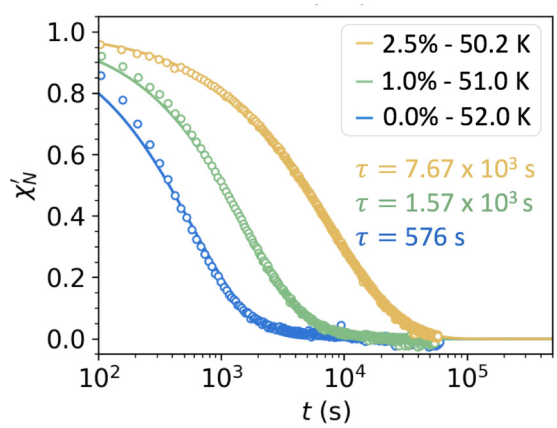

FIG. 7. The value of $\chi'(t)$ measured in the 2.5%, 1.0%, and 0.0% samples is plotted over an extended measurement time of 20 h. The data were fitted using the stretched exponential function, with fitted lifetime shown.

In Fig. 7, extended time-resolved AC susceptibility measurements are shown, demonstrating that the data tend to χ'_f and that the stretched exponential produces a good fit, allowing us to extract values of τ and β. The inclusion of the stretching parameter β is necessary to fit the data and gives an indication of the spread of lifetimes present in the sample. There are a number of possible explanations as to why the samples may display a distribution of lifetimes. For example, the effects of demagnetization would cause the magnetic field to be inhomogeneous throughout the sample, which alters the stability of the skyrmion state [44]. It has previously been demonstrated that metastable skyrmion lifetime varies with field [24]. It is also possible that a more complex metastable skyrmion decay model could account for the required stretching parameter: measurements of the relaxation of the equilibrium state have also shown nonexponential behavior [45,46]. In our measurements, we found β to fall within the range of 0.4 ± 0.04, 0.6 ± 0.08, and 0.5 ± 0.03 in the 2.5%, 1.0%, and 0.0% samples, respectively. The uncertainty here represents the spread of values fitted across all temperatures in each sample; there was no clear dependence of β with temperature.

The lifetime of the metastable skyrmion state can be expected to reach a minimum at the lowest temperature extent of the equilibrium skyrmion state T_s, which we estimate to be 4 K below T_c in all samples. Our choice to use T_s in Arrhenius's law in Eq. (2) instead of T_c, as done in previous studies [18], was to provide realistic values of a and τ_0 based on where the lifetime should be shortest. Carrying out the analysis with different values of T_s does alter the values of a and τ_0, but the relative value of each between the samples remains the same, such that our conclusions are independent of the choice of T_s.

To simulate the loss of metastable skyrmion population as the sample is cooled, we derived the following model. We begin with the expression for a population of metastable skyrmions decaying over time t with a temperature-dependent lifetime $\tau(T)$, as shown in (A1). Unlike a standard exponential function which is self-similar, when $\beta \neq 1$, the shape of a stretched exponential function changes with time. To account for this, we consider the population decay during the cooling process as a series of time steps with duration Δt, each starting at a time $t_n = n\Delta t$. For a single time step, this

gives

$$\frac{S_{n+1}}{S_n} = \frac{\exp\left[-\left(\frac{t_n+\Delta t}{\tau(T)}\right)^{\beta}\right]}{\exp\left[-\left(\frac{t_n}{\tau(T)}\right)^{\beta}\right]}. \tag{A2}$$

It follows that the final population S_0 after N time steps is a product series,

$$S_0 = S_i \prod_{n=1}^{N} \exp\left[\left(\frac{t_n}{\tau(T)}\right)^{\beta} - \left(\frac{t_n+\Delta t}{\tau(T)}\right)^{\beta}\right], \tag{A3}$$

$$S_0 = S_i \exp\left[\sum_{n=1}^{N}\left(\frac{t_n}{\tau(T)}\right)^{\beta} - \left(\frac{t_n+\Delta t}{\tau(T)}\right)^{\beta}\right], \tag{A4}$$

where S_i is the initial population before cooling commences. We now define the sum inside of the exponential function to be $g(t)$ and take the limit as $\Delta t \to 0$,

$$\lim_{\Delta t\to 0} g(t) = \lim_{\Delta t\to 0}\sum_{n=1}^{N}\left(\frac{t_n}{\tau(T)}\right)^{\beta} - \lim_{\Delta t\to 0}\sum_{n=1}^{N}\left(\frac{t_n+\Delta t}{\tau(T)}\right)^{\beta}. \tag{A5}$$

Performing a Taylor expansion of the second term around $\Delta t = 0$ yields

$$\lim_{\Delta t\to 0} g(t) = \lim_{\Delta t\to 0}\sum_{n=1}^{N}\left(\frac{t_n}{\tau(T)}\right)^{\beta} - \lim_{\Delta t\to 0}\sum_{n=1}^{N}\left[\left(\frac{t_n}{\tau(T)}\right)^{\beta} + \beta\frac{\Delta t}{t_n}\left(\frac{t_n}{\tau(T)}\right)^{\beta}\right] + \mathcal{O}^2. \tag{A6}$$

The higher-order terms of Δt^2 are infinitesimally small as $\Delta t \to 0$, leaving

$$\lim_{\Delta t\to 0} g(t) = -\lim_{\Delta t\to 0}\sum_{n=1}^{N}\beta\frac{\Delta t}{t_n}\left(\frac{t_n}{\tau(T)}\right)^{\beta}, \tag{A7}$$

$$\lim_{\Delta t\to 0} g(t) = -\beta\int_0^{t_f}\frac{1}{t}\left(\frac{t}{\tau(T)}\right)^{\beta} dt, \tag{A8}$$

where t_f is the time at the end of the cooling process. Finally, we substitute back into our equation for S_0 to find an expression for the population of metastable skyrmions as a function of time,

$$S_0 = S_i \exp\left[-\beta\int_0^{t_f}\frac{1}{t}\left(\frac{t}{\tau(T)}\right)^{\beta} dt\right]. \tag{A9}$$

In our analysis, we assume that the lifetime depends upon the temperature according to our modified Arrhenius's law,

$$\tau(T) = \tau_0 \exp\left[a\left(\frac{T_s - T}{T}\right)\right], \tag{A10}$$

where T_s is the lowest extent of the equilibrium skyrmion phase in temperature. With a linear cooling rate, $k < 0$, starting at $T = T_s$, we can write $T = T_s + kt$. We substitute Eq. (A10) into Eq. (A9) and perform a change in variables from t to T to reveal the dependence of S_0 on the cooling rate k,

$$S_0 = S_i \exp\left[\int_{T_s}^{T_f}\frac{-\beta}{T - T_s}\left(\frac{T - T_s}{k\tau_0\exp\left[a\frac{T_s - T}{T}\right]}\right)^{\beta} dT\right]. \tag{A11}$$

[1] U. K. Rößler, A. N. Bogdanov, and C. Pfleiderer, Spontaneous skyrmion ground states in magnetic metals, Nature (London) **442**, 797 (2006).

[2] N. Nagaosa and Y. Tokura, Topological properties and dynamics of magnetic skyrmions, Nat. Nanotechnol. **8**, 899 (2013).

[3] S. Mühlbauer, B. Binz, F. Jonietz, C. Pfleiderer, A. Rosch, A. Neubauer, R. Georgii, and P. Böni, Skyrmion lattice in a chiral magnet, Science **323**, 915 (2009).

[4] A. Neubauer, C. Pfleiderer, B. Binz, A. Rosch, R. Ritz, P. G. Niklowitz, and P. Böni, Topological Hall Effect in the *A* Phase of MnSi, Phys. Rev. Lett. **102**, 186602 (2009).

[5] W. Münzer, A. Neubauer, T. Adams, S. Mühlbauer, C. Franz, F. Jonietz, R. Georgii, P. Böni, B. Pedersen, M. Schmidt, A. Rosch, and C. Pfleiderer, Skyrmion lattice in the doped semiconductor $Fe_{1-x}Co_xSi$, Phys. Rev. B **81**, 041203(R) (2010).

[6] X. Z. Yu, Y. Onose, N. Kanazawa, J. H. Park, J. H. Han, Y. Matsui, N. Nagaosa, and Y. Tokura, Real-space observation of a two-dimensional skyrmion crystal, Nature (London) **465**, 901 (2010).

[7] H. Wilhelm, M. Baenitz, M. Schmidt, U. K. Rößler, A. A. Leonov, and A. N. Bogdanov, Precursor Phenomena at the Magnetic Ordering of the Cubic Helimagnet FeGe, Phys. Rev. Lett. **107**, 127203 (2011).

[8] X. Z. Yu, N. Kanazawa, Y. Onose, K. Kimoto, W. Z. Zhang, S. Ishiwata, Y. Matsui, and Y. Tokura, Near room-temperature formation of a skyrmion crystal in thin-films of the helimagnet FeGe, Nat. Mater. **10**, 106 (2011).

[9] A. Chacon, L. Heinen, M. Halder, A. Bauer, W. Simeth, S. Mühlbauer, H. Berger, M. Garst, A. Rosch, and C. Pfleiderer, Observation of two independent skyrmion phases in a chiral magnetic material, Nat. Phys. **14**, 936 (2018).

[10] K. Karube, J. S. White, D. Morikawa, C. D. Dewhurst, R. Cubitt, A. Kikkawa, X. Yu, Y. Tokunaga, T. Arima, H. M. Rønnow, Y. Tokura, and Y. Taguchi, Disordered skyrmion phase stabilized by magnetic frustration in a chiral magnet, Sci. Adv. **4**, eaar7043 (2018).

[11] T. Yokouchi, S. Hoshino, N. Kanazawa, A. Kikkawa, D. Morikawa, K. Shibata, T. Arima, Y. Taguchi, F. Kagawa, N. Nagaosa, and Y. Tokura, Current-induced dynamics of skyrmion strings, Sci. Adv. **4**, eaat1115 (2018).

[12] Y. Tokunaga, X. Z. Yu, J. S. White, H. M. Rønnow, D. Morikawa, Y. Taguchi, and Y. Tokura, A new class of chiral materials hosting magnetic skyrmions beyond room temperature, Nat. Commun. **6**, 7638 (2015).

[13] S. Seki, X. Z. Yu, S. Ishiwata, and Y. Tokura, Observation of skyrmions in a multiferroic material, Science **336**, 198 (2012).

[14] J. Iwasaki, M. Mochizuki, and N. Nagaosa, Current-induced skyrmion dynamics in constricted geometries, Nat. Nanotechnol. **8**, 742 (2013).

[15] K. Karube, J. S. White, N. Reynolds, J. L. Gavilano, H. Oike, A. Kikkawa, F. Kagawa, Y. Tokunaga, H. M. Rønnow, Y. Tokura, and Y. Taguchi, Robust metastable skyrmions and their triangular-square lattice structural transition in a high-temperature chiral magnet, Nat. Mater. **15**, 1237 (2016).

[16] K. Karube, J. S. White, D. Morikawa, M. Bartkowiak, A. Kikkawa, Y. Tokunaga, T. Arima, H. M. Rønnow, Y. Tokura, and Y. Taguchi, Skyrmion formation in a bulk chiral magnet at zero magnetic field and above room temperature, Phys. Rev. Mater. **1**, 074405 (2017).

[17] D. Morikawa, X. Yu, K. Karube, Y. Tokunaga, Y. Taguchi, T. Arima, and Y. Tokura, Deformation of topologically-protected supercooled skyrmions in a thin plate of chiral magnet $Co_8Zn_8Mn_4$, Nano Lett. **17**, 1637 (2017).

[18] H. Oike, A. Kikkawa, N. Kanazawa, Y. Taguchi, M. Kawasaki, Y. Tokura, and F. Kagawa, Interplay between topological and thermodynamic stability in a metastable magnetic skyrmion lattice, Nat. Phys. **12**, 62 (2016).

[19] T. Nakajima, H. Oike, A. Kikkawa, E. P. Gilbert, N. Booth, K. Kakurai, Y. Taguchi, Y. Tokura, F. Kagawa, and T. Arima, Skyrmion lattice structural transition in MnSi, Sci. Adv. **3**, e1602562 (2017).

[20] F. Kagawa, H. Oike, W. Koshibae, A. Kikkawa, Y. Okamura, Y. Taguchi, N. Nagaosa, and Y. Tokura, Current-induced viscoelastic topological unwinding of metastable skyrmion strings, Nat. Commun. **8**, 1332 (2017).

[21] P. Milde, D. Köhler, J. Seidel, L. M. Eng, A. Bauer, A. Chacon, J. Kindervater, S. Mühlbauer, C. Pfleiderer, S. Buhrandt *et al.*, Unwinding of a skyrmion lattice by magnetic monopoles, Science **340**, 1076 (2013).

[22] Y. Okamura, F. Kagawa, S. Seki, and Y. Tokura, Transition to and from the skyrmion lattice phase by electric fields in a magnetoelectric compound, Nat. Commun. **7**, 12669 (2016).

[23] L. J. Bannenberg, H. Wilhelm, R. Cubitt, A. Labh, M. P. Schmidt, E. Lelièvre-Berna, C. Pappas, M. Mostovoy, and A. O. Leonov, Multiple low-temperature skyrmionic states in a bulk chiral magnet, npj Quantum Mater. **4**, 11 (2019).

[24] J. Wild, T. N. G. Meier, S. Pöllath, M. Kronseder, A. Bauer, A. Chacon, M. Halder, M. Schowalter, A. Rosenauer, J. Zweck *et al.*, Entropy-limited topological protection of skyrmions, Sci. Adv. **3**, e1701704 (2017).

[25] S. S. P. Parkin, M. Hayashi, and L. Thomas, Magnetic domain-wall racetrack memory, Science **320**, 190 (2008).

[26] A. B. Kolton, A. Rosso, T. Giamarchi, and W. Krauth, Creep dynamics of elastic manifolds via exact transition pathways, Phys. Rev. B **79**, 184207 (2009).

[27] P. Chauve, T. Giamarchi, and P. Le Doussal, Creep and depinning in disordered media, Phys. Rev. B **62**, 6241 (2000).

[28] W. Kleemann, J. Rhensius, O. Petracic, J. Ferré, J. P. Jamet, and H. Bernas, Modes of Periodic Domain Wall Motion in Ultrathin Ferromagnetic Layers, Phys. Rev. Lett. **99**, 097203 (2007).

[29] C. Dhital, L. DeBeer-Schmitt, D. P. Young, and J. F. DiTusa, Unpinning the skyrmion lattice in MnSi: Effect of substitutional disorder, Phys. Rev. B **99**, 024428 (2019).

[30] A. Štefančič, S. H. Moody, T. J. Hicken, M. T. Birch, G. Balakrishnan, S. A. Barnett, M. Crisanti, J. S. O. Evans, S. J. R. Holt, K. J. A. Franke *et al.*, Origin of skyrmion lattice phase splitting in Zn-substituted Cu_2OSeO_3, Phys. Rev. Mater. **2**, 111402(R) (2018).

[31] Y. Okamura, F. Kagawa, M. Mochizuki, M. Kubota, S. Seki, S. Ishiwata, M. Kawasaki, Y. Onose and Y. Tokura, Microwave magnetoelectric effect via skyrmion resonance modes in a helimagnetic multiferroic, Nat. Commun. **4**, 2391 (2013).

[32] M. Garst, J. Waizner, and D. Grundler, Collective spin excitations of helices and magnetic skyrmions: Review and perspectives of magnonics in non-centrosymmetric magnets, J. Phys. D: Appl. Phys. **50**, 293002 (2017).

[33] M. Mochizuki and S. Seki, Dynamical magnetoelectric phenomena of multiferroic skyrmions, J. Phys.: Condens. Matter **27**, 503001 (2015).

[34] I. Stasinopoulos, S. Weichselbaumer, A. Bauer, J. Waizner, H. Berger, M. Garst, C. Pfleiderer and D. Grundler, Linearly polarized GHz magnetization dynamics of spin helix modes in the ferrimagnetic insulator Cu_2OSeO_3, Sci. Rep. **7**, 7037 (2017).

[35] Y. Onose, Y. Okamura, S. Seki, S. Ishiwata, and Y. Tokura, Observation of Magnetic Excitations of Skyrmion Crystal in a Helimagnetic Insulator Cu_2OSeO_3, Phys. Rev. Lett. **109**, 037603 (2012).

[36] A. Bauer and C. Pfleiderer, Magnetic phase diagram of MnSi inferred from magnetization and ac susceptibility, Phys. Rev. B **85**, 214418 (2012).

[37] A. Bauer and C. Pfleiderer, Magnetic relaxation phenomena in the chiral magnet $Fe_{1-x}Co_xSi$: An ac susceptibility study, Phys. Rev. B **94**, 134433 (2016).

[38] A. A. Omrani, J. S. White, K. Prša, I. Živković, H. Berger, A. Magrez, Y.-H. Liu, J. H. Han, and H. M. Rønnow, Exploration of the helimagnetic and skyrmion lattice phase diagram in Cu_2OSeO_3 using magnetoelectric susceptibility, Phys. Rev. B **89**, 064406 (2014).

[39] T. Adams, A. Chacon, M. Wagner, A. Bauer, G. Brandl, B. Pedersen, H. Berger, P. Lemmens, and C. Pfleiderer, Long-Wavelength Helimagnetic Order and Skyrmion Lattice Phase in Cu_2OSeO_3, Phys. Rev. Lett. **108**, 237204 (2012).

[40] D. C. Johnston, Stretched exponential relaxation arising from a continuous sum of exponential decays, Phys. Rev. B **74**, 184430 (2006).

[41] L. Desplat, D. Suess, J.-V. Kim, and R. L. Stamps, Thermal stability of metastable magnetic skyrmions: Entropic narrowing and significance of internal eigenmodes, Phys. Rev. B **98**, 134407 (2018).

[42] J. Romhányi, J. van den Brink, and I. Rousochatzakis, Entangled tetrahedron ground state and excitations of the magnetoelectric skyrmion material Cu_2OSeO_3, Phys. Rev. B **90**, 140404(R) (2014).

[43] O. Janson, I. Rousochatzakis, A. A. Tsirlin, M. Belesi, A. A. Leonov, U. K. Rößler, J. van den Brink, and H. Rosner, The quantum nature of skyrmions and half-skyrmions in Cu_2OSeO_3, Nat. Commun. **5**, 5376 (2014).

[44] T. Reimann, A. Bauer, C. Pfleiderer, P. Böni, P. Trtik, A. Tremsin, M. Schulz, and S. Mühlbauer, Neutron diffractive imaging of the skyrmion lattice nucleation in MnSi, Phys. Rev. B **97**, 020406(R) (2018).

[45] I. Levatić, V. Šurija, H. Berger, and I. Živković, Dissipation processes in the insulating skyrmion compound Cu_2OSeO_3, Phys. Rev. B **90**, 224412 (2014).

[46] F. Qian, H. Wilhelm, A. Aqeel, T. T. M. Palstra, A. J. E. Lefering, E. H. Brück, and C. Pappas, Phase diagram and magnetic relaxation phenomena in Cu_2OSeO_3, Phys. Rev. B **94**, 064418 (2016).

[47] T. M. Birch, "Increased lifetime of metastable Skyrmions by controlled Doping", Durham University, doi:10.15128/r12514nk51w (2019).